Materials Advances

ROYAL SOCIETY OF CHEMISTRY

PAPER

View Article Online
View Journal | View Issue

Cite this: *Mater. Adv.*, 2024, 5, 8701

DNAsome with self-boosting ROS generation *via* tumour acidosis for enhanced and targeted chemodynamic cancer therapy†

Gowtham Raj, Justin Prasad, Tamraparni Ghosh, Vasudev D. S., Athul V. B., Joyraj Kalita, Devu B. Kumar and Reji Varghese *

The anticancer efficacy of chemodynamic therapy (CDT) is significantly reduced owing to the mild acidic nature of the tumour microenvironment (TME). Typically, Fenton catalysts require a strong acidic microenvironment for effective radical generation at the tumour site. Hence the development of new strategies to achieve efficient Fenton reactions by increasing the acidity of the TME is highly demanded for the advancement of CDT-based cancer treatment. Herein, we demonstrate that the loading of the pH-regulator tamoxifen (**TAM**) into a CDT nanoagent (**DNA1some**) could significantly boost the efficiency of CDT action by increasing the acidity at the TME. The integration of nucleolin specific aptamer DNA (**DNA2**) onto the surface of **DNA1some** (**DNA1some/TAM/DNA2**) permitted the targeted internalization of the nanoformulation selectively into cancer cells, and consequently, a very efficient Fenton reaction was demonstrated inside the cancer cells selectively, which reduced the "off-target" toxicity of the nanoformulation to the surrounding normal cells. Enhanced cytotoxicity was observed for the **TAM**-loaded **DNA1some** compared to **DNA1some** and **TAM** alone, which was attributed to the very efficient Fenton reaction by **DNA1some** due to the increase in acidity caused by the release of **TAM**. Hence, the pH-regulator-loaded CDT-active DNAsome can potentially overcome the intrinsically insufficient acidity of the TME for enabling efficient Fenton reactions.

Received 14th August 2024,
Accepted 3rd October 2024

DOI: 10.1039/d4ma00822g

rsc.li/materials-advances

Introduction

Chemodynamic therapy (CDT) is an emerging non-invasive therapeutic approach for the treatment of cancer.[1–6] It involves the use of a transition metal as a catalyst for the conversion of endogenous hydrogen peroxide (H_2O_2) present in the tumor microenvironment (TME) to yield highly oxidizing hydroxyl radicals ($^{\bullet}OH$) *via* Fenton/Fenton-like reactions. The oxidative nature of $^{\bullet}OH$ disrupts redox homeostasis and ultimately leads to cell death.[7–9] Compared to other conventional therapeutic approaches, such as chemo, radiation, photothermal and photodynamic, the therapeutic action of CDT solely depends on the abundantly available transition metal as a catalyst and endogenous H_2O_2. Hence, CDT does not require any complicated instrumentation, which makes it a superior therapeutic choice over other conventional strategies for cancer treatment.[10,11]

Ideally, the Fenton reaction requires an acidic pH (pH 3.0–5.0) for the efficient generation of $^{\bullet}OH$.[12–14] However, because the pH range of the TME is only 6.5–6.9, the efficiency of the Fenton reaction has been found to be poor in the TME, which in turn reduces the therapeutic performance of CDT-based cancer therapy.[15,16] Off-target toxicity to the surrounding normal tissues due to non-targeted accumulation of metal catalysts is another challenge associated with CDT-based cancer therapy. Hence the development of novel strategies to achieve efficient Fenton reactions by increasing the acidity of the TME in a targeted fashion is highly demanded for the advancement of CDT-based cancer treatment.

DNA-based nanostructures have recently emerged as potential nanocarriers for the delivery of metal ions (Fenton catalyst) to the TME because of their excellent biocompatibility, water solubility and, most importantly, their strong non-covalent interactions with metal ions through their negatively charged phosphate backbone and with nucleobases.[17,18] Among the various metal ions, Cu^{2+} has received particular attention as a Fenton catalyst owing to its beneficial characteristics.[19–22] For instance, Cu^{2+} exhibits good catalytic activity even in weakly acidic conditions.[23–26] Moreover, Cu^{2+} reacts with endogenous glutathione (GSH) to form Cu^{+}, which is the catalytically active form of copper for the Fenton reaction.[27,28] Hence the active form of copper would be generated preferably inside cancer cells due to the high concentration of GSH

School of Chemistry Indian Institute of Science Education and Research (IISER), Thiruvananthapuram, Trivandrum 695551, Kerala, India.
E-mail: reji@iisertvm.ac.in

† Electronic supplementary information (ESI) available. See DOI: https://doi.org/10.1039/d4ma00822g

inside cancer cells compared to the normal cells. This leads to the preferential activation of the Fenton reaction inside cancer cells, which would also be less likely to occur inside normal cells. This potentially reduces the off-target toxicity to the surrounding healthy cells. It should also be noted that Cu^{2+} not only produces catalytically active Cu^{+} but also downregulates GSH (antioxidant), with both reactions highly beneficial for efficient CDT. In addition, the surface of DNA nanostructures can be integrated with cell-targeting DNA aptamers *via* sequence-specific DNA hybridization, allowing the targeted delivery of the Fenton catalyst into the cancerous cells selectively.[29–39]

Very recently, we reported a class of DNA amphiphiles consisting of a Cu^{2+}–salen complex as a hydrophobic Fenton reaction centre and ssDNA as the hydrophilic segment.[40] Self-assembly of the amphiphile (**DNA1**) resulted in the formation of CDT-active vesicles (**DNA1some**) having a Cu^{2+}-based Fenton reaction centre as the membrane of the vesicle and hydrophilic ssDNA as the shell. One of the challenges associated with CDT for cancer therapy is the poor yield of the Fenton reaction due to the nearly neutral pH range around the TME (pH 6.5–6.9).[16] In this work, we wanted to improve the CDT efficacy of **DNA1some** by increasing the acidity of the TME. Tamoxifen (**TAM**) is a popular anti-oestrogen drug and is extensively used in treatment of oestrogen receptor-positive breast cancer.[12,41] It has also been shown that **TAM** can inhibit the function of mitochondrial complex I and thereby increase the AMP to ATP ratio, which triggers the AMP-activated protein kinase signalling pathway.[12] This in turn causes an enhancement in the rate of glycolysis reactions and lactate generation, which leads to a significant decrease in the pH in the TME. Hence, we envisioned that the delivery of the pH-regulator **TAM** along with the CDT-active **DNA1some** into cancer cells would be a promising approach to boost the efficiency of CDT by decreasing the pH of the TME by the action **TAM**.

Herein, we report on the formulation of **TAM**-loaded **DNA1some** (**DNA1some/TAM**) and investigations into the therapeutic performance of the nanoformulation for targeted CDT-based cancer therapy using MDA-MB-231 as a representative cancer cell (Scheme 1). The self-assembly of **DNA1** in the presence of **TAM** resulted in the formation of the **TAM**-loaded **DNA1some** (**DNA1some/TAM**), where the hydrophobic **TAM** most likely resides in the hydrophobic membrane of **DNA1some**. The DNA-based surface addressability of **DNA1some** was used for the integration of nucleolin-targeting DNA aptamer (**DNA2**) *via* sequence-specific DNA hybridization to form **DNA1some/TAM/DNA2**. Nucleolin is known to be overexpressed on the surfaces of several cancer cells, including MDA-MB-231.[42] Following the nucleolin receptor-mediated endocytosis, **DNA1some/TAM/DNA2** disassembles inside the lysosome and leads to the release of **TAM** and free Cu^{2+} at the cytoplasm. Free Cu^{2+} is then *in situ* reduced to Cu^{+} by the cellular GSH, and undergoes a Fenton reaction using endogenous H_2O_2 to produce $^{\bullet}OH$. Enhanced cytotoxicity was observed for **DNA1some/TAM/DNA2** when compared to **DNA1some** alone. The enhanced cytotoxicity of **DNA1some/TAM/DNA2** was attributed to the efficient Fenton reaction due to the more acidic TME caused by the action of **TAM**.

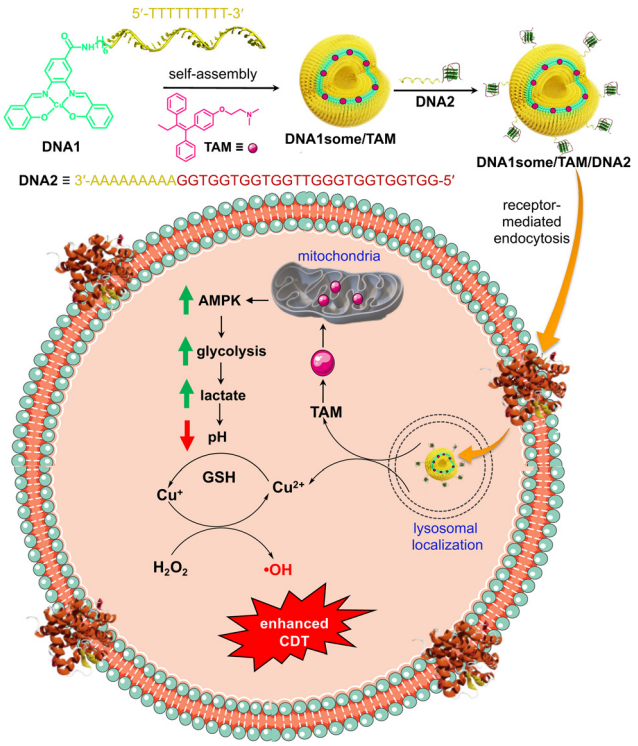

Scheme 1 Schematic of the self-assembly of **DNA1** in the presence of **TAM** for the formation of **TAM**-loaded **DNA1some** (**DNA1some/TAM**). Integration of aptamer DNA (**DNA2**) onto the surface of **DNA1some/TAM** is shown. Targeted cellular internalization of **DNA1some/TAM/DNA2** *via* nucleolin receptor-mediated endocytosis, followed by pH-assisted enhanced chemodynamic therapy, is also shown.

Results and discussion

Synthesis and characterization of the **DNA1** amphiphile were reported in our recent report.[40] Specifically, the amphiphilicity-driven self-assembly of **DNA1** in aqueous medium (pH 7.0) led to the formation of CDT-active vesicular nanostructures (**DNA1some**), which were fully characterized using various spectroscopic, microscopic, and light scattering analyses, with the details of the analysis procedures also reported in our recent paper.[40] The self-assembly of **DNA1** (5 μM) in the presence of the pH-regulator **TAM** (10 μM) resulted in the formation of **TAM**-loaded **DNA1some** (**DNA1some/TAM**). The loading of **TAM** in the hydrophobic membrane of **DNA1some** was probed by UV-vis absorption spectroscopy by comparing the absorbance of a concentration-matched solution of free **TAM** with the **TAM** concentration of the filtrate of **DNA1some/TAM** (Fig. 1a).

The absorption spectrum of free **TAM** (10 μM in MeOH) showed three major bands at 210, 250, and 290 nm. On the other hand, a significant reduction in the intensity of the absorption bands was observed for the filtrate obtained after the centrifugal filtration of **DNA1some/TAM** (**DNA1some** = 5 μM in H_2O, **TAM** = 10 μM in MeOH) using a molecular weight cut-off filter. This reduction in intensity for the filtrate of **DNA1some/TAM** clearly indicated the efficient loading of **TAM** into the hydrophobic membrane of **DNA1some**. The loading efficiency of **TAM** was calculated to be ~80%. Transmission

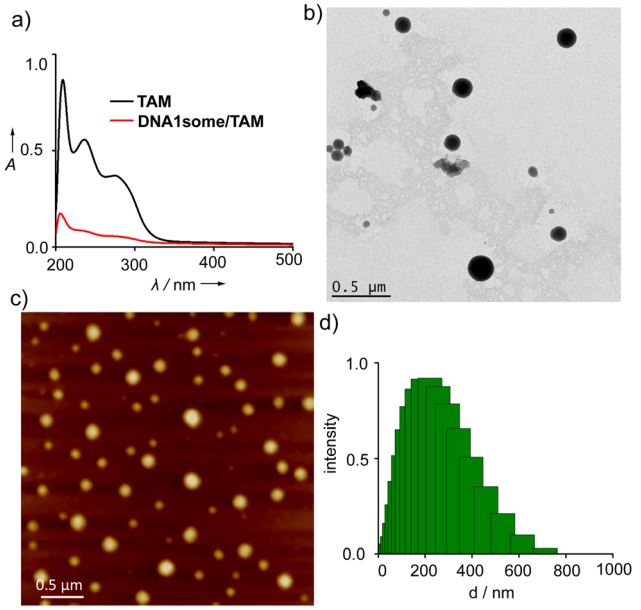

Fig. 1 (a) Comparison of the absorption spectra of free **TAM** and **TAM** present in the filtrate of **DNA1some/TAM**. (b) AFM and (c) TEM images of **DNA1some/TAM**. (d) DLS size distribution of **DNA1some/TAM** aggregates.

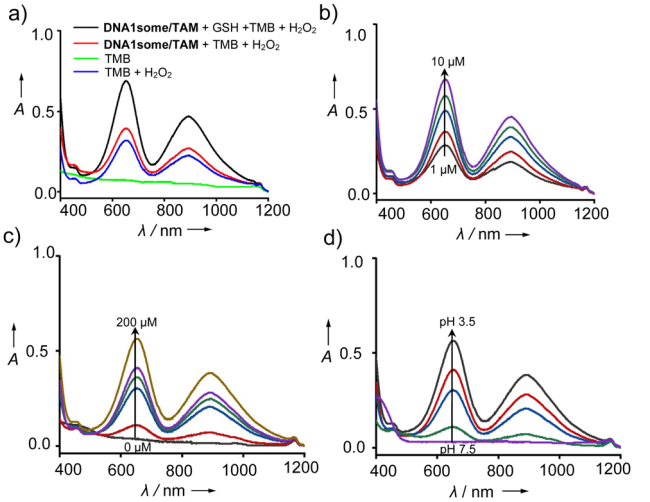

Fig. 2 (a) Comparison of the absorption spectra for the H_2O_2-mediated oxidation of TMB-catalysed **DNA1some/TAM** under various reaction conditions. Absorption spectra of TMB oxidation mediated by **DNA1some/TAM** at varying (b) concentrations of **DNA1some**, (c) concentrations of H_2O_2, and (d) pH.

electron microscopy (TEM) (Fig. 1b) and atomic force microscopy (AFM) (Fig. 1c) analyses were applied to reveal the vesicular morphology of **DNA1some/TAM** (**DNA1some** = 5 μM in H_2O, **TAM** = 10 μM in MeOH), indicating that the vesicular morphology of **DNA1some** was retained even after loading **TAM**. The average diameter of the vesicles of **DNA1some/TAM** was found to be ~200 nm, which was nearly the same as that of the diameter of **DNA1some** alone, suggesting that the loading of **TAM** did not affect the diameter of **DNA1some**. In support of the microscopic analyses, dynamic light scattering (DLS) analysis of **DNA1some/TAM** showed a unimodal distribution of spherical aggerates with an average diameter of ~200 nm (Fig. 1d). These results collectively allowed concluding that the self-assembly of **DNA1** in the presence of **TAM** resulted in the formation of **TAM**-loaded **DNA1some**, with **TAM** most likely residing in the hydrophobic membrane of **DNA1some**.

After the characterization of **DNA1some/TAM**, we evaluated the peroxidase-like (POD) activity of **DNA1some/TAM**, and found it was due to the presence of Cu^{2+} in the salen complex. According to our design, Cu^{2+} is *in situ* reduced to Cu^{+} by GSH at acidic pH, and then reacts with H_2O_2 to form $^{\bullet}OH$.[40] Tetramethylbenzidine (TMB) was chosen as the substrate to probe the POD activity of **DNA1some/TAM**. For this, **DNA1some/TAM** ([**DNA1some**] = 20 μM, [**TAM**] = 10 μM) was treated with TMB (500 μM) in the presence of H_2O_2 (200 μM) and GSH (20 μM) at pH 5.0, and the emergence of the peak corresponding to oxidized TMB (ox-TMB) at 650 nm was monitored. As shown in Fig. 2a, the most intense peak of ox-TMB was observed for **DNA1some/TAM** and H_2O_2 in the presence of GSH compared to **DNA1some/TAM** and H_2O_2 in the absence of GSH, revealing the excellent POD activity of **DNA1some/TAM** in the presence of GSH. Moreover, **DNA1some/TAM** exhibited good activity even at a low concentration (1 μM) of **DNA1some** (Fig. 2b). As expected, the catalytic activity was found to increase with the increase in H_2O_2 concentration (Fig. 2c).

Next, we evaluated the effect of pH on the catalytic activity of **DNA1some/TAM**. Typically, the Fenton reaction requires acidic pH 3.0–5.0 to facilitate the catalytic action. When **DNA1some/TAM** was incubated in sodium acetate buffer with different pH values, the absorption peak of ox-TMB at 650 nm was found to increase with the decrease in pH. The maximum POD-like activity was observed at pH 3.5, while the lowest activity was observed at pH 7.5. These results strongly suggest that **DNA1some/TAM** exhibits excellent POD-like activity in an acidic pH environment (Fig. 2d).

After demonstrating the encapsulation of **TAM** inside **DNA1some** and the POD-mimicking activity of **DNA1some/TAM**, the cellular internalization of **DNA1some/TAM** was studied using MDA-MB-231 as a representative cancer cell. Towards this, a G-quadruplex-based cell-targeting aptamer **DNA2** (5′-GGTGG TGGTGGTTGGGTGGTGGTGGAAAAAAAAA-3′) was integrated onto the surface of **DNA1some/TAM** *via* sequence-specific DNA hybridization to yield **DNA1some/TAM/DNA2**. The **DNA2** integrated on the surface of **DNA1some/TAM** can then act as a targeting ligand, targeting the membrane-overexpressed nucleolin proteins on the surface of MDA-MB-231 cells and allowing the selective internalization of **DNA1some/TAM** into MDA-MB-231 cells compared to healthy cells. In order to monitor the cellular internalization, **DNA2** was fluorescently labelled with FAM at the 5′-end (**DNA3**) and the green fluorescence of **DNA3** was used to investigate the internalization of the nanoformulation. For this, **DNA1some/TAM/DNA3** ([**DNA1**] = 20 μM, [**TAM**] = 20 μM, [**DNA3**] = 1 μM) was incubated with MDA-MB-231 cells for 12 h and the internalization of the nanoformulation was studied by confocal laser scanning microscopy (CLSM). The CLSM images showed a strong overlay of the green fluorescence

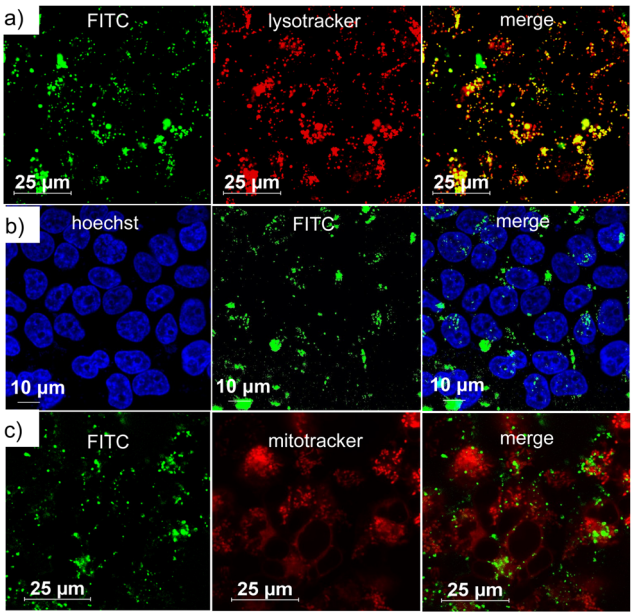

Fig. 3 CLSM images of **DNA1some/TAM/DNA3**-treated MDA-MB-231 cells: (a) lysosomal, (b) nuclear and (c) mitochondrial colocalization of **DNA1some/TAM/DNA3**.

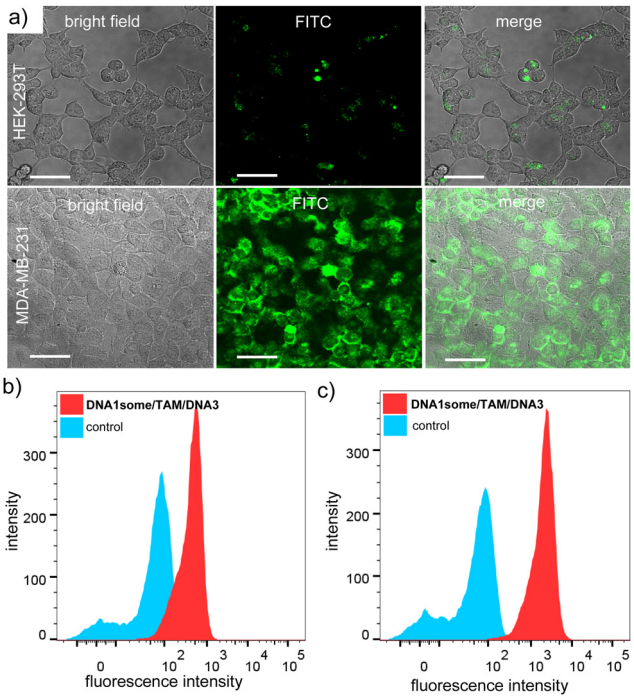

Fig. 4 (a) CLSM images of **DNA1some/TAM/DNA3**-treated HEK-293T and MDA-MB-231 cells and (b) and (c) corresponding FACS analyses for HEK-293T and MDA-MB-231 cells.

of **DNA1some/TAM/DNA3** with the red fluorescence of lysotracker from the lysosome of the cells. This clearly suggests the lysosomal entrapment of **DNA1some/TAM/DNA3** immediately after nucleolin-targeted receptor-mediated endocytosis (Fig. 3a). In support of this, the corresponding line analyses revealed the excellent colocalization of **DNA1some/TAM/DNA3** with lysosome, with a high Pearson's correlation coefficient of 0.724 (Fig. S4, ESI†).

In order to understand whether the nanoformulation undergoes localization in any other cell organelles, such as mitochondria and nucleus, colocalization experiments were performed after staining the nucleus and the mitochondria. The nucleus of MDA-MB-231 cells was stained with Hoechst (blue fluorescence) and mitochondria with MitoTracker deep red (red fluorescence). The corresponding CLSM images clearly revealed no colocalization of the green fluorescence of **DNA1some/TAM/DNA3** with the blue fluorescence of Hoechst (Fig. 3b) and the red fluorescence of MitoTracker deep red (Fig. 3c). In accordance with these, very low Pearson's correlation coefficients were observed for the colocalization of the mitochondria (0.149) and nucleus (0.012) (Fig. S5 and S6, ESI†). These results verified the specific lysosomal entrapment of **DNA1some/TAM/DNA3** and its subsequent degradation at the lysosome to release free Cu^{2+} and **TAM**. The selective internalization of **DNA1some/TAM/DNA3** into nucleolin overexpressed cancer cells was then studied by comparing the cellular internalization efficiency of the nanoformulation between MDA-MB-231 (nucleolin overexpressed cancer cells) and HEK-293T (healthy cells) cell lines.[42] The CLSM analyses disclosed an intense green fluorescence for the **DNA1some/TAM/DNA3**-treated MDA-MB-231 cells, whereas only a negligible green fluorescence was associated with the **DNA1some/TAM/DNA3**-treated HEK-293T cells (Fig. 4a). This clearly indicates the selective internalization of the nanoformulation into nucleolin overexpressed cancer cells.

In support of this, the corresponding fluorescence-activated cell sorting (FACS) analyses revealed the high mean fluorescence intensity (MFI) shift for the **DNA1some/TAM/DNA3**-treated MDA-MB-231 cells (2153) when compared to the corresponding HEK-293T cells (436) (Fig. 4b). Furthermore, the cellular internalization of **DNA1some/TAM/DNA3** was found to be directly proportional to the relative expression level of nucleolin on the cell membrane. In order to validate this, the efficiency of the cellular internalization of **DNA1some/TAM/DNA3** was studied using three different cell lines having different nucleolin expression levels, namely MCF-7 (high nucleolin expression), HeLa (medium nucleolin expression), and HEK-293T (low nucleolin expression) cells.[43] Accordingly, the CLSM analyses revealed the highest fluorescence intensity for MCF-7 cells, moderate intensity for HeLa cells, and the lowest intensity for HEK-293T cells; clearly revealing that the cellular internalization of **DNA1some/TAM/DNA3** was directly proportional to the expression level of nucleolin on the membrane of the cells (Fig. S7, ESI†).

The pH-regulator **TAM** was incorporated into the nanoformulation to decrease the pH of the TME, and thereby enhance the efficacy of CDT action. To investigate the ability of **DNA1some/TAM/DNA2** to decrease intracellular pH, MDA-MB-231 cells were incubated with **DNA1some/TAM/DNA2** ([**DNA1**] = 20 μM, [**TAM**] = 20 μM, [**DNA2**] = 1 μM) and the decrease in intracellular pH was probed using a fluorescent pH indicator, namely 2′,7′-bis-(2-carboxyethyl)-5-(and-6)-carboxyfluorescein acetoxy-methyl ester (BCECF); whereby a decrease in the

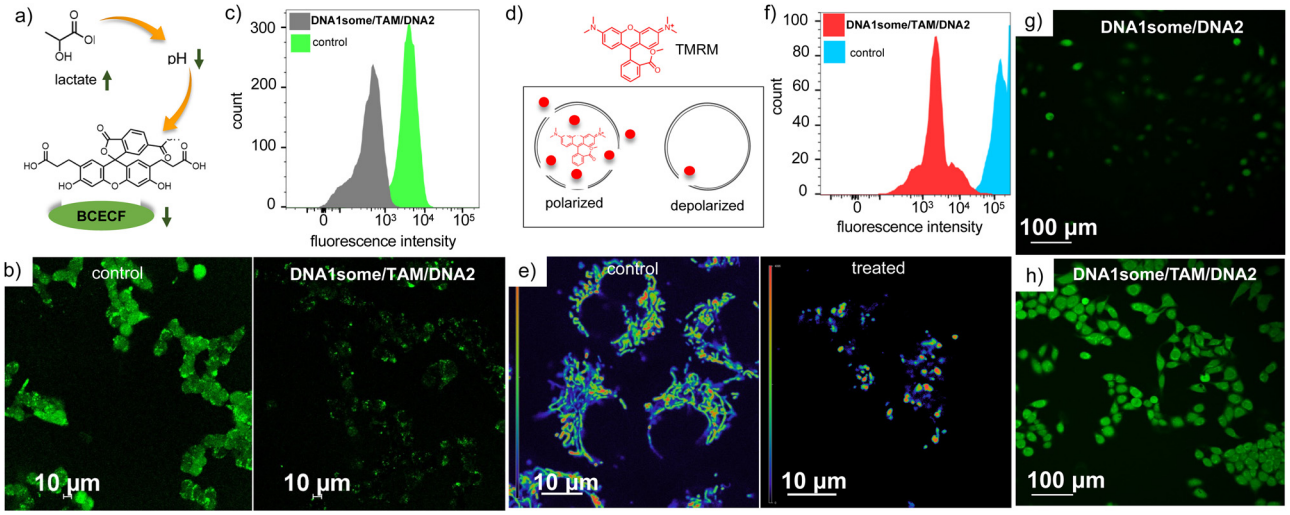

Fig. 5 (a) Chemical reactions involved in the BCECF-AM assay for the measurement of intracellular pH. (b) CLSM images of **DNA1some/TAM/DNA2**-treated MDA-MB-231 cells stained with BCECF-AM and (c) the corresponding FACS analyses. (d) Schematic of the principle of TMRM assay. (e) CLSM images of **DNA1some/TAM/DNA2**-treated MDA-MB-231 cells stained with TMRM and (f) the corresponding FACS analyses. CLSM images of (g) **DNA1some/DNA2-** and (h) **DNA1some/TAM/DNA2**-treated MDA-MB-231 cells stained with DCFH-DA.

fluorescence intensity of BCECF-AM would be indicative of the decrease in intracellular pH. In accordance with our design, the CLSM images of **DNA1some/TAM/DNA2**-treated MDA-MB-231 cells showed a lower green fluorescence intensity compared to the untreated control cells (Fig. 5b). This result indicates that **TAM** released from **DNA1some/TAM/DNA2** acts as an inhibitor of mitochondrial complex I, which enhances glycolysis and the lactate content and increases the acidity of TME. This was subsequently confirmed and quantified by FACS analyses, which displayed a lower MFI shift for **DNA1some/TAM/DNA2**-treated cells (502) compared to the untreated control cells (3889) (Fig. 5c).

We have previously reported that **DNA1some** alone could not induce any mitochondrial damage.[40] In order to understand whether the *in situ*-released **TAM** can cause any mitochondrial damage as a result of the inhibition of mitochondrial complex I, a tetramethylrhodamine methyl ester perchlorate (TMRM) assay was performed on **DNA1some/TAM/DNA2** ([**DNA1some**] = 20 μM, [**TAM**] = 20 μM, [**DNA2**] = 1 μM)-treated MDA-MB-231 cells. TMRM binds strongly to healthy and polarized mitochondria, whereas it binds weakly to unhealthy and depolarized mitochondria and hence a reduction in the florescence intensity of TMRM is an indication of damaged mitochondria. A significant decrease in TMRM fluorescence was observed for **DNA1some/TAM/DNA2**-treated cells when compared to the corresponding untreated control cells, revealing mitochondrial damage due to the release of **TAM** (Fig. 5e). This was further supported through FACS analyses, which exhibited a significant reduction in the MFI shift value for the **DNA1some/TAM/DNA2**-treated cells (3780) compared to the corresponding untreated controlled cells (129676) (Fig. 5f).

Having achieved a **TAM**-induced acidic TME inside the MDA-MB-231 cells, we evaluated the CDT action of **DNA1some/TAM/DNA2** ([**DNA1some**] = 20 μM, [**TAM**] = 20 μM, [**DNA2**] = 1 μM) using 2,7-dichlorofluorescein-diacetate (DCFH-DA) as a fluorescent probe for the detection of ROS. This was achieved by probing the formation of green fluorescent 2,7-dichlorofluorescein (DCF) upon the reaction of ROS with DCFH-DA. As shown in Fig. 5g and h, the **DNA1some/TAM/DNA2**-treated MDA-MB-231 cells showed stronger DCF green fluorescence than the **DNA1some/DNA2**-treated cells. FACS analyses also revealed a high MFI shift for the **DNA1some/TAM/DNA2**-treated cells (620) compared to the **DNA2/DNA1some**-treated cells (99). These results indicate the enhanced ROS generation for the **DNA1some/TAM/DNA2**-treated cells due to the increased acidity induced by the release of **TAM**.

Subsequently, we tested the cytotoxicity of **DNA1some/TAM/DNA2** ([**DNA1some**] = 20 μM, [**TAM**] = 20 μM, [**DNA2**] = 1 μM) *via* a methyl thiazolyl tetrazolium (MTT) assay. As expected, enhanced cytotoxicity was observed for **DNA1some/TAM/DNA2** compared to **DNA1some** and **TAM**, revealing the synergetic combination of **DNA1some** and **TAM** (Fig. 6a). Cell deaths of 28% and 54% were observed for the **DNA1some-** and **TAM**-treated cells, respectively. On the other hand, a higher cell death of 74% was observed for the **DNA1some/TAM/DNA2**-treated sample. Very interestingly, only negligible cytotoxicity (13%) was observed for the **DNA1some/TAM/DNA2**-treated HEK-293T cells, indicating the high selectivity of the nanoformulation due to the presence of the aptamer DNA (**DNA2**) on the surface of the nanoformulation (Fig. 6b). The cytotoxicity was further visualized by calcein-AM/propidium iodide (PI) co-staining assay. Calcein-AM stains and imparts green fluorescence for viable cells, whereas PI stains the dead cells and imparts red fluorescence.[44–46] In accordance with the MTT assay, the **DNA1some/TAM/DNA2** ([**DNA1some**] = 20 μM, [**TAM**] = 20 μM, [**DNA2**] = 1 μM)-treated MDA-MB-231 cells exhibited mostly red fluorescent cells compared to the **DNA1some-** and **TAM**-treated cells, further confirming the excellent cytotoxicity of **DNA1some/TAM/DNA2** (Fig. 6c).

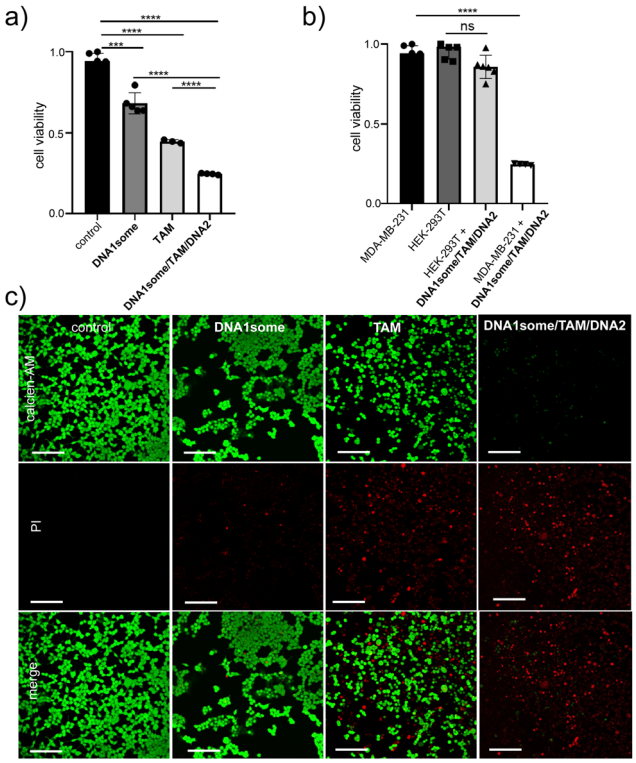

Fig. 6 (a) MTT assay of various CDT agents-treated MDA-MB-231 cells. (b) Comparison of the MTT assays for **DNA1some/TAM/DNA2**-teated HEK-293T and MDA-MB-231 cells demonstrating the selectivity of **DNA1some/TAM/DNA2**. (c) Calcein-AM/PI live-dead cell assay of **DNA1some/TAM/DNA2**-treated MDA-MB-231 cells. Scale bars correspond to 100 μm.

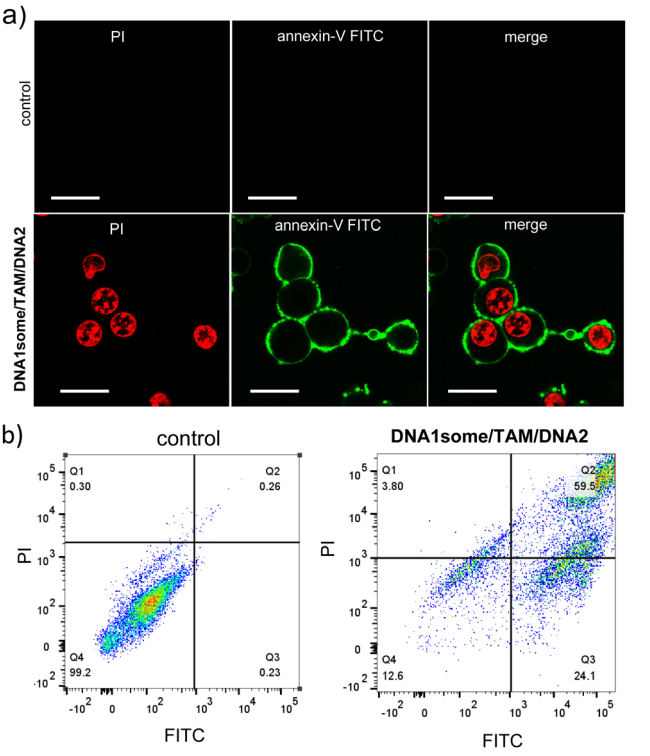

Fig. 7 (a) Annexin V-FITC/PI assay of **DNA1some/TAM/DNA2**-treated MDA-MB-231 cells and (b) the corresponding FACS analyses. Scale bars correspond to 25 μm.

Subsequently, an annexin V-FITC (AV)/PI assay was performed to understand the mechanism of cell death. Annexin V-FITC binds to the cell membrane during the early stages of apoptosis and gives rise to green fluorescence around the cell membrane. In contrast, PI binds to the nucleus at the late stage of apoptosis and gives rise to red fluorescence. For this, MDA-MB-231 cells were treated with **DNA1some/TAM/DNA2** ([**DNA1some**] = 20 μM, [**TAM**] = 20 μM, [**DNA2**] = 1 μM) for 12 h and analysed by CLSM and FACS. The CLSM images clearly showed green and red fluorescence at the membrane and the nucleus of the cells, respectively, implying the apoptotic pathway of cell death (Fig. 7a). In accordance with this, the FACS studies showed the shift of the cell population to the quadrant corresponding to the apoptotic pathway (Fig. 7b). These results allowed concluding that **DNA1some/TAM/DNA2** induces cell death *via* the apoptotic pathway.

After demonstrating the *in vitro* performance of **DNA1some/TAM/DNA2**, we studied the efficiency of the CDT agent in a multicellular tumour spheroid model using a 3D cell culture. The 3D-multicellular tumour spheroid mimics the *in vivo* tumour, and it undergoes proliferation in all directions similar to malignant tumours. In 3D cell culture, the cells clump together to form a stable 3D spheroid-like structure, wherein the communication and signalling between the cells are maximized, leading to efficient proliferation and invasion over time.[47–49] In our study of triple-negative human breast cancer cells, MDA-MB-231 was used to prepare tumour 3D spheroids using the hanging drop method.[50,51] The invasion potential of the spheroids was then studied in the presence of **DNA1some/TAM/DNA2** to understand the effect on the spheroid invasion. For this, 3D spheroids were incubated with **DNA1some/TAM/DNA2** ([**DNA1some**] = 20 μM, [**TAM**] = 20 μM, [**DNA2**] = 1 μM) at 37 °C for 24 h. Untreated spheroids were considered as the controls and showed the maximum invasion potential as they exhibited migration in all directions. On the other hand, the invasion was significantly reduced for the **DNA1some/TAM/DNA2**-treated sample due to the combined therapeutic actions. A nearly nil invasion index was observed for the **DNA1some/TAM/DNA2**-treated sample compared to the untreated sample, which showed an invasion index of 1.92 ± 0.5 (Fig. 8).

Conclusions

In summary, we report a CDT nanoagent loaded with a pH regulator for the improvement of CDT action by decreasing the pH at the TME for targeted cancer therapy. Self-assembly of a DNA amphiphile containing a Fenton reaction centre as the hydrophobic segment resulted in the formation of CDT-active DNAsome. One of the unique features of DNAsome is the dense surface decoration of ssDNA with a defined sequence, which permitted the integration of the DNA aptamer for nucleolin onto the surface of the DNAsome *via* sequence-specific DNA hybridization. The aptamer-decorated DNAsome exhibited

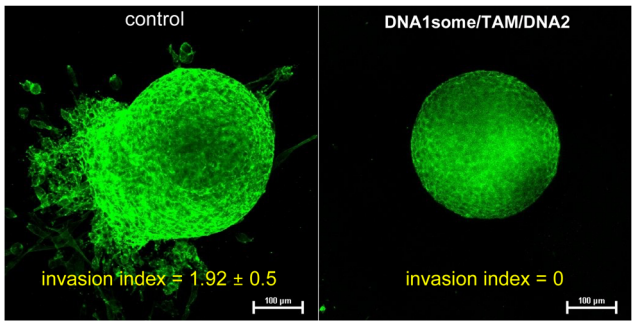

Fig. 8 CLSM images of the **DNA2/TAM/DNA1some**-treated MDA-MB-231 3D spheroids (left) and the corresponding untreated control spheroids (right).

excellent targeted internalization towards nucleolin overexpressed cancer cells, whereas negligible internalization was observed for normal cell lines, indicating the significantly reduced "off-target" toxicity to the surrounding normal cells. The cytotoxicity of the CDT agent was found to be significantly increased by the loading of the pH regulator and excellent targeted cytotoxicity was shown by the nanoformulation when compared to the CDT agent alone. This was attributed to the efficient Fenton reaction due to the acidic TME caused by the action of the pH regulator. We presented a simple and promising strategy to increase the efficiency of CDT action of CDT-active DNAsome by the non-covalent incorporation of a pH regulator into the hydrophobic membrane of the DNAsome. We strongly feel that this strategy would definitely help in the advancement of CDT-based targeted cancer therapy and will also encourage other researchers in this area to explore this approach for the advancement of cancer therapy in general.

Author contributions

The manuscript was written through the contributions of all authors. All authors have given approval to the final version of the manuscript.

Data availability

The data supporting this article have been included as part of the ESI.†

Conflicts of interest

There are no conflicts to declare.

Acknowledgements

Financial support from SERB (CRG/2022/002612) is gratefully acknowledged. The help of Sarika Mohan S. is acknowledged for the FACS analyses.

References

1 Z. Tang, Y. Liu, M. He and W. Bu, *Angew. Chem., Int. Ed.*, 2019, **58**, 946–956.
2 K. Wei, Y. Wu, X. Zheng, L. Ouyang, G. Ma, C. Ji and M. Yin, *Angew. Chem., Int. Ed.*, 2024, **63**, e202404395.
3 C. Zheng, Z. Wang, H. Xu, H. Huang, X. Tao, Y. Hu, Y. He, Z. Zhang and X. Huang, *Small Methods*, 2024, **8**, 2301099.
4 B. Zhao, Z. Ma, S. Ding, Y. Cao, J. Du, L. Zeng, Y. Hu, J. Zhou, X. Zhang, X. Bian and G. Tian, *Adv. Funct. Mater.*, 2023, **33**, 2306328.
5 L. Zhang, C.-X. Li, S.-S. Wan and X.-Z. Zhang, *Adv. Healthcare Mater.*, 2022, **11**, 2101971.
6 A. Silswal and A. L. Koner, *Chem. Commun.*, 2023, **59**, 1769–1772.
7 M. Peng, E. Ju, Y. Xu, Y. Wang, S. Lv, D. Shao, H. Wang, Y. Tao, Y. Zheng and M. Li, *NPG Asia Mater.*, 2022, **14**, 95.
8 H. Lin, Y. Chen and J. Shi, *Chem. Soc. Rev.*, 2018, **47**, 1938–1958.
9 C. Jia, Y. Guo and F.-G. Wu, *Small*, 2022, **18**, 2103868.
10 C. Cao, X. Wang, N. Yang, X. Song and X. Dong, *Chem. Sci.*, 2022, **13**, 863–889.
11 L.-S. Lin, J. Song, L. Song, K. Ke, Y. Liu, Z. Zhou, Z. Shen, J. Li, Z. Yang, W. Tang, G. Niu, H.-H. Yang and X. Chen, *Angew. Chem., Int. Ed.*, 2018, **57**, 4902–4906.
12 L. Shi, Y. Wang, C. Zhang, Y. Zhao, C. Lu, B. Yin, Y. Yang, X. Gong, L. Teng, Y. Liu, X. Zhang and G. Song, *Angew. Chem., Int. Ed.*, 2021, **60**, 9562–9572.
13 S. Fu, R. Yang, L. Zhang, W. Liu, G. Du, Y. Cao, Z. Xu, H. Cui, Y. Kang and P. Xue, *Biomaterials*, 2020, **257**, 120279.
14 Y. Liu, J. Wu, Y. Jin, W. Zhen, Y. Wang, J. Liu, L. Jin, S. Zhang, Y. Zhao, S. Song, Y. Yang and H. Zhang, *Adv. Funct. Mater.*, 2019, **29**, 1904678.
15 B. Lin, H. Chen, D. Liang, W. Lin, X. Qi, H. Liu and X. Deng, *ACS Appl. Mater. Interfaces*, 2019, **11**, 11157–11166.
16 B. Ma, S. Wang, F. Liu, S. Zhang, J. Duan, Z. Li, Y. Kong, Y. Sang, H. Liu, W. Bu and L. Li, *J. Am. Chem. Soc.*, 2019, **141**, 849–857.
17 L. Lin, J. Yu, H. Lu, Z. Wei, Z. Chao, Z. Wang, W. Wu, H. Jiang and L. Tian, *Chem. Commun.*, 2021, **57**, 1734–1737.
18 M. Li, C. Wang, Z. Di, H. Li, J. Zhang, W. Xue, M. Zhao, K. Zhang, Y. Zhao and L. Li, *Angew. Chem., Int. Ed.*, 2019, **58**, 1350–1354.
19 C. Liu, Y. Chen, J. Zhao, Y. Wang, Y. Shao, Z. Gu, L. Li and Y. Zhao, *Angew. Chem., Int. Ed.*, 2021, **60**, 14324–14328.
20 C. Liu, S. Jia, L. Tu, P. Yang, Y. Wang, S. Ke, W. Shi and S. Ye, *ACS Biomater. Sci. Eng.*, 2022, **8**, 1942–1955.
21 C.-K. Sun, Y.-H. Wang, Y.-L. Chen, T.-Y. Lu, H.-Y. Chen, S.-C. Pan, P.-C. Chen, M.-Y. Liao and J. Yu, *Sci. Rep.*, 2022, **12**, 18729.
22 W.-X. Zhang, Y.-N. Hao, Y.-R. Gao, Y. Shu and J.-H. Wang, *ACS Appl. Mater. Interfaces*, 2021, **13**, 38127–38137.
23 M. Chen, S. Zhao, J. Zhu, E. Feng, F. Lv, W. Chen, S. Lv, Y. Wu, X. Peng and F. Song, *ACS Appl. Mater. Interfaces*, 2022, **14**, 20682–20692.
24 Q. Li, J. Yu, L. Lin, Y. Zhu, Z. Wei, F. Wan, X. Zhang, F. He and L. Tian, *ACS Appl. Mater. Interfaces*, 2023, **15**, 16482–16491.

25 W. B. Direrssa, T.-C. Kan, J. Chang, G. Getachew, S. Ochirbat, S. Kizhepat, A. Wibrianto, A. Rasal, H.-A. Chen, A. V. Ghule, T.-H. Chou and J.-Y. Chang, *ACS Appl. Mater. Interfaces*, 2024, **16**, 24172–24190.
26 Q. Yu, J. Zhou, Y. Liu, X. Q. Li, S. Li, H. Zhou, B. Kang, H.-Y. Chen and J.-J. Xu, *Adv. Healthcare. Mater.*, 2023, **12**, 2301429.
27 Y.-N. Hao, W.-X. Zhang, Y.-R. Gao, Y.-N. Wei, Y. Shu and J.-H. Wang, *J. Mater. Chem. B*, 2021, **9**, 250–266.
28 Y. You, H. Liu, J. Zhu, Y. Wang, F. Pu, J. Ren and X. Qu, *Chem. Sci.*, 2022, **13**, 7829–7836.
29 Q. Li, F. Wang, L. Shi, Q. Tang, B. Li, X. Wang and Y. Jin, *ACS Appl. Mater. Interfaces*, 2022, **14**, 37280–37290.
30 L. Zhang, R. Abdullah, X. Hu, H. Bai, H. Fan, L. He, H. Liang, J. Zou, Y. Liu, Y. Sun, X. Zhang and W. Tan, *J. Am. Chem. Soc.*, 2019, **141**, 4282–4290.
31 C. Ji, H. Li, L. Zhang, P. Wang, Y. Lv, Z. Sun, J. Tan, Q. Yuan and W. Tan, *Angew. Chem., Int. Ed.*, 2022, **61**, e202200237.
32 J. Tan, H. Li, X. Hu, R. Abdullah, S. Xie, L. Zhang, M. Zhao, Q. Luo, Y. Li, Z. Sun, Q. Yuan and W. Tan, *Chem*, 2019, **5**, 1775–1792.
33 Y. Ouyang, M. Fadeev, P. Zhang, R. Carmieli, J. Li, Y. S. Sohn, O. Karmi, R. Nechushtai, E. Pikarsky, C. Fan and I. Willner, *ACS Nano*, 2022, **16**, 18232–18243.
34 W. Song, P. Song, Y. Sun, Z. Zhang, H. Zhou, X. Zhang and P. He, *ACS Biomater. Sci. Eng.*, 2021, **7**, 5165–5174.
35 W. Xuan, Y. Xia, T. Li, L. Wang, Y. Liu and W. Tan, *J. Am. Chem. Soc.*, 2020, **142**, 937–944.
36 C. Yao, H. Qi, X. Jia, Y. Xu, Z. Tong, Z. Gu and D. Yang, *Angew. Chem., Int. Ed.*, 2022, **61**, e202113619.
37 Q. Tang, Q. Li, L. Shi, W. Liu, B. Li and Y. Jin, *Nanoscale Horiz.*, 2023, **8**, 1106–1112.
38 W. Tang, L. Han, X. Lu, Z. Wang, F. Liu, Y. Li, S. Liu, S. Liu, R. Tian, J. Liu and B. Ding, *ACS Appl. Mater. Interfaces*, 2021, **13**, 20974–20981.
39 J. Y. Lee, Q. Yang, X. Chang, H. Wisniewski, T. R. Olivera, M. Saji, S. Kim, D. Perumal and F. Zhang, *J. Mater. Chem. B*, 2022, **10**, 7460–7472.
40 G. Raj, A. P. Vasantha, V. D. Sreekumar, A. V. Beena, V. K. K. Dommeti, H. Perozhy, A. T. Jose, S. Khurana and R. Varghese, *Adv. Healthcare Mater.*, 2024, 2400256.
41 V. C. Jordan, *Nat. Rev. Drug Discovery*, 2003, **2**, 205–213.
42 J. He, T. Peng, Y. Peng, L. Ai, Z. Deng, X.-Q. Wang and W. Tan, *J. Am. Chem. Soc.*, 2020, **142**, 2699–2703.
43 S. Sun, Y. Yang, Z. Gao, H. Jiang, L. Ye, Y. Lai, Z. Shen and Z.-S. Wu, *ACS Appl. Mater. Interfaces*, 2022, **14**, 45201–45216.
44 A. Konieva, V. Deineka, K. Diedkova, D. Aguilar-Ferrer, M. Lyndin, G. Wennemuth, V. Korniienko, S. Kyrylenko, A. Lihachev, V. Zahorodna, I. Baginskiy, E. Coy, O. Gogotsi, A. Blacha-Grzechnik, W. Simka, I. Kube-Golovin, I. Iatsunskyi and M. Pogorielov, *ACS Appl. Mater. Interfaces*, 2024, **16**, 43302–43316.
45 A. Joe, P. Manivasagan, J. K. Park, H.-W. Han, S.-H. Seo, T. Thambi, V. H. Giang Phan, S. A. Kang, J. Conde and E.-S. Jang, *ACS Nano*, 2024, **18**, 19581–19596.
46 T. Xia, Z. Xia, P. Tang, J. Fan and X. Peng, *J. Am. Chem. Soc.*, 2024, **146**, 12941–12949.
47 A. Aung, S. K. Davey, J. Theprungsirikul, V. Kumar and S. Varghese, *Adv. Healthcare Mater.*, 2023, **12**, 2201842.
48 L. Yu, Y. Xu, M. Al-Amin, S. Jiang, M. Sample, A. Prasad, N. Stephanopoulos, P. Šulc and H. Yan, *J. Am. Chem. Soc.*, 2023, **145**, 27336–27347.
49 M. L. Janssen, T. Liu, M. Özel, M. Bril, H. V. Prasad Thelu and R. E. Kieltyka, *Angew. Chem., Int. Ed.*, 2024, **63**, e202314738.
50 H. NaveenaA and D. D. Bhatia, *ChemBioChem*, 2023, **24**, e202300506.
51 A. Rajwar, S. R. Shetty, P. Vaswani, V. Morya, A. Barai, S. Sen, M. Sonawane and D. Bhatia, *ACS Nano*, 2022, **16**, 10496–10508.